Activation of STIM1/Orai1-mediated SOCE in sepsis-induced myocardial depression

JINGJING YE[1,2], MENGFANG LI[1], QIAO LI[3], ZHIJUN JIA[3], XIYI HU[1], GUANGJU ZHAO[1,2], SHAOCE ZHI[1], GUANGLIANG HONG[1,2] and ZHONGQIU LU[1,2]

[1]Emergency Department; [2]Wenzhou Key Laboratory of Emergency and Disaster Medicine; [3]Ultrasound Department, The First Affiliated Hospital of Wenzhou Medical University, Wenzhou, Zhejiang 325000, P.R. China

Received February 4, 2021; Accepted February 21, 2022

DOI: 10.3892/mmr.2022.12775

Abstract. Unbalanced Ca^{2+} homeostasis serves an essential role in the occurrence and development of septic myocardial injury. However, the mechanism of Ca^{2+} homeostasis in septic myocardial depression is poorly understood due to the complexity of Ca^{2+} transporters in excitable cells. It was therefore hypothesized that cardiac dysfunction, myocardial injury and cardiac apoptosis in septic myocardial depression are associated with elevated intracellular Ca^{2+} concentrations caused by stromal interaction molecule 1 (STIM1)/Orai calcium release-activated calcium modulator 1 (Orai1)-mediated store-operated Ca^{2+} entry (SOCE). A septic myocardial depression model was established using the cecal ligation and puncture operation (CLP) in mice and was simulated in H9C2 cells via lipopolysaccharide (LPS) stimulation. Cardiac function, myocardial injury, cardiac apoptosis and the expression levels of Bax, Bcl-2, STIM1 and Orai1 were quantified *in vivo* at 6, 12 and 24 h. Changes in the intracellular Ca^{2+} concentration, SOCE and the distribution of STIM1 were assessed *in vitro* within 6 h. The morphological changes of heart tissue were observed by hematoxylin-eosin staining. Myocardial cellular apoptosis was determined by TUNEL method. The expression of Bax, Bcl-2, STIM1 and Orai1 were visualized by western blot. Cytosolic calcium concentration and SOCE were evaluated by confocal microscopy. The results demonstrated that cardiac contractile function was significantly reduced at 6 h and morphological changes in cardiac tissues, as well as the myocardial apoptosis rate, were markedly increased at 6, 12 and 24 h following CLP. mRNA and protein expression levels of Bax/Bcl-2 were significantly enhanced at 6 and 12 h and glycosylation of Orai1 in the myocardium of septic mice was significantly increased at 6 h following CLP. The intracellular Ca^{2+} concentration, SOCE, was significantly increased at 1-2 h and the clustering and distribution of STIM1 were markedly changed in H9C2 cells at 1 and 2 h. These findings suggested that myocardial dysfunction, cardiac injury and myocardial depression may be related to increased intracellular Ca^{2+} concentration resulting from STIM1/Orai1-mediated SOCE, which may provide a potential method to alleviate septic myocardial depression.

Correspondence to: Professor Zhongqiu Lu, Emergency Department, The First Affiliated Hospital of Wenzhou Medical University, 2 Fuxue Lane, Wenzhou, Zhejiang 325000, P.R. China
E-mail: lzq_640815@163.com

Key words: sepsis, myocardial, Ca^{2+}, store-operated Ca^{2+} entry

Introduction

Sepsis is life-threatening organ dysfunction caused by an uncontrollable immune response induced by infection (1). Among the multi-organ dysfunction syndromes induced by sepsis, 40% of patients have reduced cardiac function and 20% have cardiac dysfunction (2). Sepsis-induced myocardial depression contributes to the prognosis of patients with sepsis and exploring the pathogenesis of sepsis-induced cardiac depression may alleviate the prognosis of these patients (3). The mechanism of cardiac depression may result from structural effects due to cardiomyocyte death, as well as functional effects caused by cardiac dysfunction. Calcium (Ca^{2+}) homeostasis is essential for normal cardiac excitation contraction coupling (4). Ca^{2+} also serves an essential role in the signalling pathways associated with cellular termination, including induction of apoptosis and damage to structural proteins (5,6). Lipopolysaccharide (LPS) efficiently increases the intracellular Ca^{2+} concentration in cardiomyocytes (7) and disruption of Ca^{2+} homeostasis reduces dystrophin, actin and myosin expression, but increases the expression of calpain. It also leads to decreases in left ventricular ejection fraction (LVEF) and left ventricular fractional shortening (LVFS) (8). Moreover, inhibitors of the sarcoplasmic reticulum (SR) Ca-ATPase and Ca^{2+} chelators decrease cellular Ca^{2+} levels, which may reduce the cardiac apoptosis induced by LPS (9). However, the transient Ca^{2+} concentrations responsible for contraction fluctuate several times a minute from 0.1 μM in the diastole period to 1-10 μM in the systole period, which does not appear to activate cellular signalling events (10). Therefore, the activation of signalling pathways by Ca^{2+} is distinct from the Ca^{2+} fluctuations responsible for normal cycles of myocardial excitation, contraction and relaxation.

Voltage-gated Ca^{2+} entry is the main source of elevated intracellular cardiac Ca^{2+} levels and originates from Ca^{2+}

influx via the plasma membrane (11). Store-operated Ca^{2+} entry (SOCE) is an additional pathway of Ca^{2+} entry originally associated with Ca^{2+} changes in unexcited cells (12-14). Neonatal and embryonic cardiomyocytes depleted of Ca^{2+} in the SR were previously demonstrated to efficiently induce Ca^{2+} influx, which was blocked by the SOCE inhibitor SKF-96365, but not the L-type Ca^{2+} channel (LTCC) blocker verapamil (15). SOCE has also been detected in adult cardiomyocytes using whole-cell patch-clamp experiments (16). However, understanding the role of SOCE in cardiomyocytes was limited until the proteins essential to this signalling pathway were discovered. SOCE is associated with stromal interaction molecule 1 (STIM1) and Orai calcium release-activated calcium modulator 1 (Orai1) (17) and the expression of STIM1 and Orai1 has also been reported in myocardium (18-20). Orai1 is a transmembrane protein of the cytomembrane and is a Ca^{2+} channel-mediated Ca^{2+} entry point from the internal environment (21). As a protein located in the cellular membrane, Orai1 does not sense changes in Ca^{2+} levels in the endoplasmic reticulum (ER) (21). The STIM1 protein is distributed mainly in the ER membrane and can sense changes to the Ca^{2+} level in the ER (22). It has been demonstrated that depletion of Ca^{2+} in the ER can induce the clustering and distribution of STIM1 to the ER-plasma membrane junctions, which subsequently mediates the activation of Orai1 (22).

Numerous studies have demonstrated the role of STIM1/Orai1-mediated SOCE in the pathogenesis of cardiac disease (23-26), especially in cardiac hypertrophy (27,28). However, to the best of our knowledge the role of STIM1/Orai1-mediated SOCE in the development of septic myocardial depression has not been reported. During septic myocardial depression, inhibition of the SR Ca-ATPase and enhanced ryanodine receptor leakage induce depletion of Ca^{2+} in the ER (29). Therefore, we hypothesize that STIM1/Orai1-mediated SOCE contributes to the pathogenesis and development of septic cardiac depression.

Materials and methods

Reagents. LPS and anti-Orai1 antibody (cat. no. SAB3500127) were purchased from Sigma-Aldrich (Merck KGaA). Antibodies for STIM1 (cat. no. ab108994) and Bax (cat. no. ab32503) were purchased from Abcam. Antibody against Bcl-2 (cat. no. 2870T) was purchased from Cell Signaling Technology, Inc. GAPDH (cat. no. BS60630) was purchased from Bioworld Technology, Inc. and secondary antibodies (cat. no. BL003A) for western blotting was purchased from Biosharp Life. TRIzol® reagent was obtained from Invitrogen (Thermo Fisher Scientific, Inc.). QuantiTect Reverse Transcription (RT) Kit and SYBR Green Master Mix were purchased from Takara Biotechnology Co., Ltd. DyLightFluor® 488-conjugated donkey anti-rabbit IgG secondary antibodies (cat. no. BYE026 was obtained from Shanghai Boyun Biotech Co., Ltd. Fluo-3AMacetoxymethyl ester (AM; cat. no. s1056) and bovine serum albumin (BSA) were purchased from Beyotime Institute of Biotechnology. Thapsigargin used for depleting SR Ca^{2+} stores (TG; cat. no. mb13319) was purchased from Dalian Melone Biotechnology Co., Ltd. and terminal deoxynucleotidyl transferase dUTP nick-end labelling (TUNEL) kits were purchased from Roche Molecular Diagnostics.

Animals. Male C57BL/6 mice (age, 8 weeks; weight, 20-25 g) were obtained from Shanghai SLAC Laboratory Animal Co., Ltd. and were raised under pathogen-free conditions at 25˚C at 50% humidity and 12-h light/dark cycles with free access to food and water. The present study was performed in accordance with the National Institutes of Health Guidelines for Care and Use of Animals (30) and was approved by the Ethics Committee of Wenzhou Medical University (Wenzhou, China).

CLP model. In total, 90 mice were randomly assigned to the following six groups: i) Sham 6 h; ii) Sham 12 h; iii) sham 24 h; iv) CLP 6 h; v) CLP 12 h; and vi) CLP 24 h. The CLP model was established as described previously (31,32). Briefly, mice were anesthetized with pentobarbital sodium (50 mg/kg intraperitoneally) and following sterilization a midline incision (1 cm) was made to expose the cecum. The cecum was ligated in half and punctured twice using an 18-gauge needle before removing a small amount of stool and placing it in the abdomen. The wound was sutured following the CLP operation. Mice in the sham group underwent a laparotomy without CLP operation. All mice were resuscitated with a subcutaneous injection of a 24 ml/kg sterile saline solution (0.9%). At the corresponding timepoint, mice were sacrificed by cervical dislocation after anaesthesia using pentobarbital sodium (50 mg/kg intraperitoneally). Death was verified by cessation of heartbeat and pupil dilation.

Survival rate. The survival rate of the mice in each group was evaluated within 72 h of the sham or CLP operation. Mice had free access to water and food and were kept under pathogen-free conditions and were monitored every 6 h. All mice were euthanasia at the end of the study.

Evaluation of cardiac function by echocardiography. Cardiac function was assessed via transthoracic echocardiographic examination. Mice were lightly anesthetized with isoflurane anaesthesia (3% induction and 1~2% maintenance). The assessment of left ventricular cardiac function was performed before and after the operation to assess the influence of CLP on cardiac function. Echocardiographic images were obtained using an echocardiography instrument equipped with a 15 MHz phased-array transducer (GE LOGIQ E9; General Electric Company). The motion mode (M-mode) images of the left ventricular dimensions were taken and the LVEF and LVFS were assessed.

Hematoxylin and eosin (H&E) staining. The hearts of the mice were harvested after the sham or CLP operations and fixed in 4% paraformaldehyde at 4˚C for 24 h. Paraffin-embedded myocardial tissues were cut into sections (5 μm). H&E staining was performed at room temperature with 0.25% hematoxylin for 10 min and 0.5% eosin for 2 min. Morphological changes were evaluated using the Olympus CKX41SF light microscope (Olympus Corporation).

TUNEL staining. Myocardial apoptosis was detected using the TUNEL method. The heart tissues were fixed in a

4% paraformaldehyde at 4˚C for 24 h. Paraffin-embedded myocardial tissues were cut into sections (5 μm) and the slides were stained with 50 μl TUNEL reagent (50 μl terminal deoxynucleotidyl transferase and 450 μl biotin-dUTP) for 60 min at 37˚C. Subsequently, the samples were incubated with 50 μl horseradish peroxidase-conjugated streptavidin solution at room temperature for 30 min and were then developed with DAB chromogenic reagent (5 μl 20X DAB + 1 μl 30% H2O2+94 μl PBS) for 5 min at room temperature. The slices were stained with haematoxylin, dehydrated by ethanol and mounted with neutral balata fixation. Representative images were taken using a light microscope. Five random fields were evaluated in each slide.

RT-quantitative (q)PCR. Total RNA was isolated from the myocardium of CLP and sham mice using TRIzol according to the manufacturer's protocol. Complementary DNA was synthesized from 1 μg total RNA using PrimeScript™ RT Master Mix (Takara Biotechnology Co., Ltd) according to the manufacturer's protocol described. qPCR was performed using the SYBR Green Master Mix (Takara Biotechnology Co., Ltd) with the CFX96 Real-Time PCR System (Bio-Rad Laboratories, Inc.). The following thermocycling conditions were used: 30 sec at 95˚C; followed by 40 cycles of 15 sec at 95˚C and 1 min at 60˚C. The primers used for qPCR were as follows: Bax forward (F), 5'-CAGTTGAAGTTGCCATCAGC-3' and reverse (R) 5'-ATGCGTCCACCAAGAAGC-3'; Bcl-2 F, 5'-GCGACGAGAGAAGTCATCC-3' and R, 5'-AGCCTGAGAGCAACCCAAT-3', STIM1 F, 5'-CCCTTCCAGATCCTTCATCA-3' and R, 5'-AAGGACTTCATGCTGGTGGT-3'; Orai1 F, 5'-GTGCCCGGTGTTAGAGAATG-3' and R, 5'-TCCCTGGTCAGCCATAAGAC-3'; and GAPDH F, 5'-AAGAGGGATGCTGCCCTTAC-3' and R, 5'-TACGGCCAAATCCGTTCACA-3'. The mRNA expression levels of the target genes were normalized to those of GAPDH and fold changes were quantified using the $2^{-\Delta\Delta Cq}$ method (33).

Western blotting. Myocardial tissues were harvested and lysed using RIPA lysis buffer (Beyotime Institute of Biotechnology). The protein concentration of the supernatant was determined using a BCA protein assay kit. Equivalent amounts of total protein (30-60 μg protein/lane) were separated via SDS-PAGE on a 8-12% gel. Subsequently, separated protein was transferred to a PVDF membrane (MilliporeSigma). After blocking with 5% non-fat milk at room temperature for 2 h, the membranes were incubated with primary antibodies against STIM1 (1:1,000), Bax (1:1,000), Bcl-2 (1:1,000), or Orai1 (1:500) at 4˚C overnight. Following the primary incubation membranes were washed with Tris-buffered saline containing 0.1% Tween-20 for three times and then incubated followed with secondary antibodies (1:5,000; cat. no. BL003A; Biosharp Life Science, Inc.) at room temperature for 2 h. Membranes were detected with an enhanced chemiluminescence kit (Thermo Fisher Scientific, Inc.) and were semi-quantified using Quantity One v4.6.6 software (Bio-Rad Laboratories, Inc.). GAPDH (cat. no. BS60630; 1:8,000; Bioworld Technology, Inc.) was used as a loading control.

Cell culture and treatment. H9C2 cells were purchased from The Cell Bank of Type Culture Collection of The Chinese Academy of Sciences. Cells were cultured in Dulbecco's Modified Eagle's Medium (Gibco; Thermo Fisher Scientific, Inc.) supplemented with 10% FBS (Gibco; Thermo Fisher Scientific, Inc.), 100 IU/ml penicillin and 100 mg/ml streptomycin at 37˚C with 5% CO_2. H9C2 cells were randomly assigned to two groups: i) Control (PBS stimulation); ii) LPS (10 μg/ml). Cells were seeded into plates at an appropriate density ($1x10^5$/ml) and incubated for 24 h before incubation with LPS or PBS for 0.5-6.0 h at 37˚C and were subsequently harvested for analysis (34).

Immunofluorescence staining. Cells from each treatment group were fixed with 4% paraformaldehyde at 4˚C for 1 h and then permeabilized with 0.5% Triton X-100 at room temperature for 10 min. After blocking with 1% BSA at 4˚C for 30 min the cells were incubated with anti-STIM1 (1:100) and anti-Orai1 (1:100) primary antibodies at 4˚C overnight. Samples were then incubated with dyLightFluor® 488-conjugated donkey anti-rabbit (1:400) or anti-mouse (1:400) IgG secondary antibody for 1 h at room temperature and cells were stained with 10 μg/ml DAPI for 7 min in the dark at room temperature. Representative images were captured using the Olympus BX51 fluorescent microscope (Olympus Corporation).

Store-operated Ca^{2+} entry in cardiomyocytes. SOCE was quantified as described previously (18). Briefly, H9C2 cells were loaded with 5 μmol/l Fluo-3/AM (excitation at 488 nm) for 40 min at 37˚C in normal Tyrode's solution (140 mmol/l NaCl, 5.4 mmol/l KCl, 1 mmol/l $MgCl_2$, 2 mmol/l $CaCl^2$, 5.5 mmol/l glucose and 5 mmol/l HEPES at pH 7.4) in the dark and LPS (10 μg/ml) was administered for 40 min at 37˚C. After dye loading, cells were washed with PBS three times within 20 min at room temperature. To prevent store refilling and deletion of intracellular Ca^{2+} stores, cells were treated with 4 μmol/l TG in Ca^{2+}-free Tyrode's solution. SOCE was triggered by the addition of 1.8 mmol/l Ca^{2+} to the solution. The cells were captured first before TG or Ca^{2+} was added. Real-time fluorescent images (all cells) were recored every 2 sec using confocal microscopy (Nikon A1; Nikon Corporation) within 1 h and were analysed using the supporting software (Nikon NIS-Elements AR 4.XX.00). The cells were still alive when the images were recorded, thus H9C2 cells were stimulated by LPS for 1-2 h (40 min dying at 37˚C, 20 min washing and 0-1 h recording at room temprature).

Statistical analysis. All experiments were performed in triplicate. Data are presented as the mean ± SD. All analyses were performed using SPSS version 16.0 software (SPSS, Inc.). Statistical significance was assessed using two-tailed unpaired Student's t-test (two groups) and one-way ANOVA followed by Tukey's post hoc test (three or more groups). $P<0.05$ was considered to indicate a statistically significant difference.

Results

Establishment of septic myocardial depression. Sepsis-induced alterations in cardiac structure and function were analysed according to the survival rate, cardiac contractility and myocardial injury. The survival rate of mice in the sham group was 100% following the CLP operation (Fig. 1A).

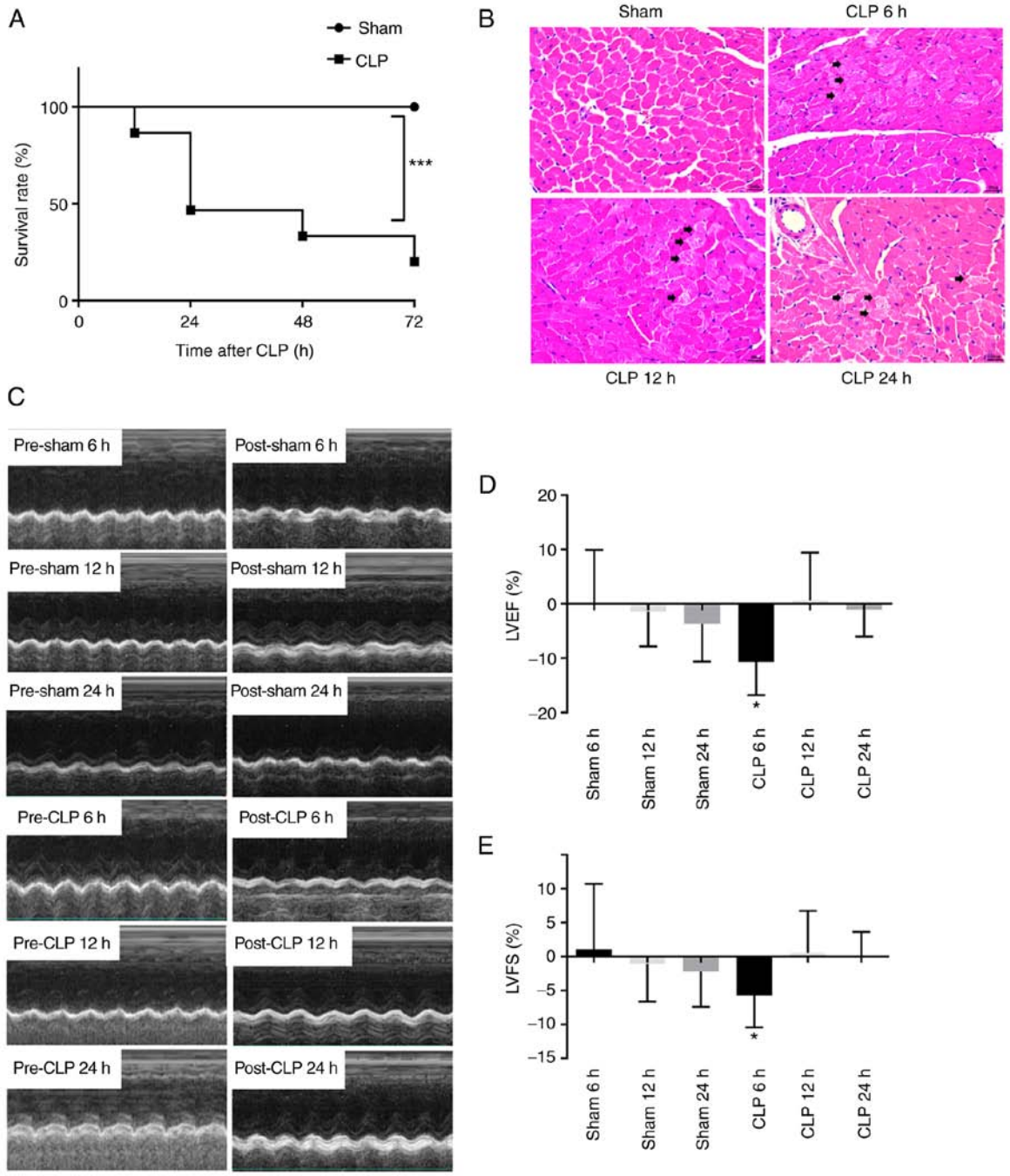

Figure 1. Survival rate, cardiac dysfunction and myocardial injury in septic mice. (A) Survival rate at 12, 24, 48 and 72 h following CLP operation (n=20 for each group). ***P<0.001 vs. sham. (B) Representative images of H&E staining. The black arrow indicate cardiomyocyte damage and loss of clear cardiac muscle cross striations (n=6 for each group). Scale bar, 20 μm. (C) Representative motion mode images. (D) LVEF. (E) LVES. Data are presented as the mean ± SEM (n=8/group). *P<0.05 vs. sham 6 h. CLP, cecal ligation and puncture operation; LVEF, left ventricle ejection fraction; LVFS, left ventricular fractional shortening.

However, compared with the sham group a marked decrease in survival rate was observed following CLP, with survival rates of 46.7% at 24 h and 20% at 72 h (vs. sham group, P<0.001). Changes in survival rate in the CLP group indicated the success of the septic animal model. Myocardial sections were stained with H&E to assess the damage to the myocardium induced by CLP. Cardiomyocytes were demonstrated to be intact and the cardiac muscle cross striations were clear in the sham group. In the CLP group, cardiomyocytes were destroyed and the cardiac muscle cross striations were no longer clear. Damage to the myocardial tissues by CLP continued following the operation (Fig. 1B). Changes in cardiac function resulting from sepsis were analysed using echocardiography. The results demonstrated significant reductions in the LVEF (10.7%) and LVES (5.7%) in the CLP group at 6 h (P<0.05) compared with the sham 6 h group (Fig. 1C-E). No significant change in the LVEF or LVES was observed at 12 and 24 h in the CLP group compared with the corresponding time-point sham group.

Myocardial apoptosis is induced in septic mice. The myocardial sections damaged by the CLP operation, as confirmed by H&E staining, were used to assess the rate of cardiomyocyte

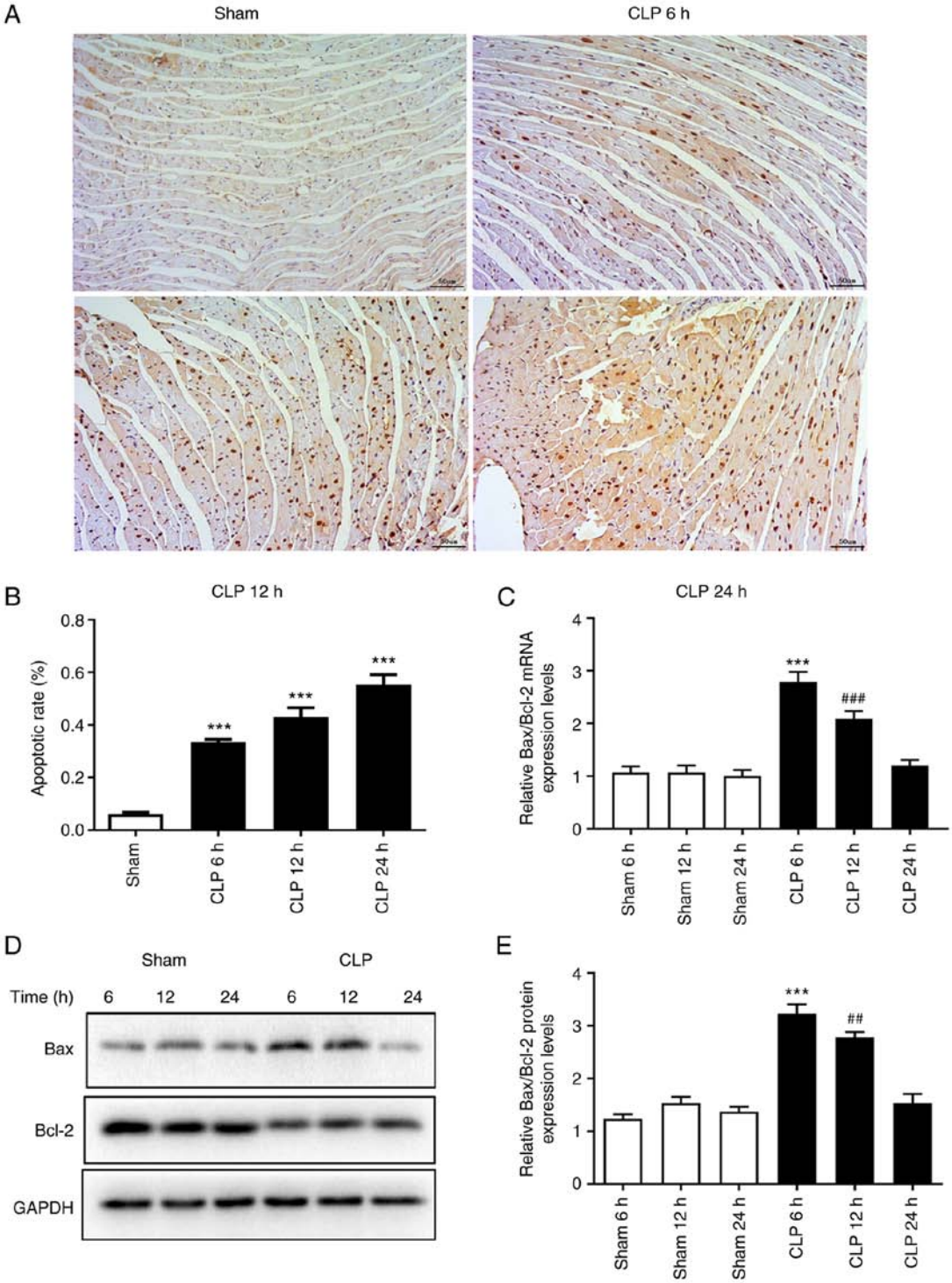

Figure 2. Induction of myocardial cellular apoptosis in septic mice. (A) Myocardial apoptotic cells were detected using TUNEL staining. Scale bar, 50 μm. (B) Apoptotic rate. ***P<0.001 vs. sham. (C) RT-qPCR analysis of Bax/Bcl-2 mRNA expression levels. (D) Representative western blotting images and (E) semi-quantification of Bax and Bcl-2 protein expression levels. Data are presented as the mean ± SEM (n=6/group). ***P<0.001 vs. sham 6 h; $^{\#\#}$P<0.01, $^{\#\#\#}$P<0.01 vs. sham 12 h. RT-qPCR, reverse transcription-quantitative PCR; CLP, cecal ligation and puncture operation.

apoptosis induced by sepsis via TUNEL staining. The rate of cardiomyocyte apoptosis was 6% in the 24 h sham group compared with 33.5% at 6 h (P<0.001), 43.1% at 12 h (P<0.001) and 55.3% at 24 h (P<0.001) following CLP, which indicated that the myocardial apoptosis rate significantly increased over time following the operation compared with the sham group (Fig. 2A and B). The mRNA and protein expression levels of apoptosis-related Bax and Bcl-2 were assessed using RT-qPCR and western blotting, respectively, to investigate the activation of sepsis-induced myocardial apoptosis. The ratio of Bax/Bcl-2 mRNA and protein expression levels were significantly increased in the CLP group at 6 (P<0.001) and 12 h (P<0.01) compared with the corresponding sham groups (Fig. 2C-E). The peak Bax/Bcl-2 ratio was observed at 6 h

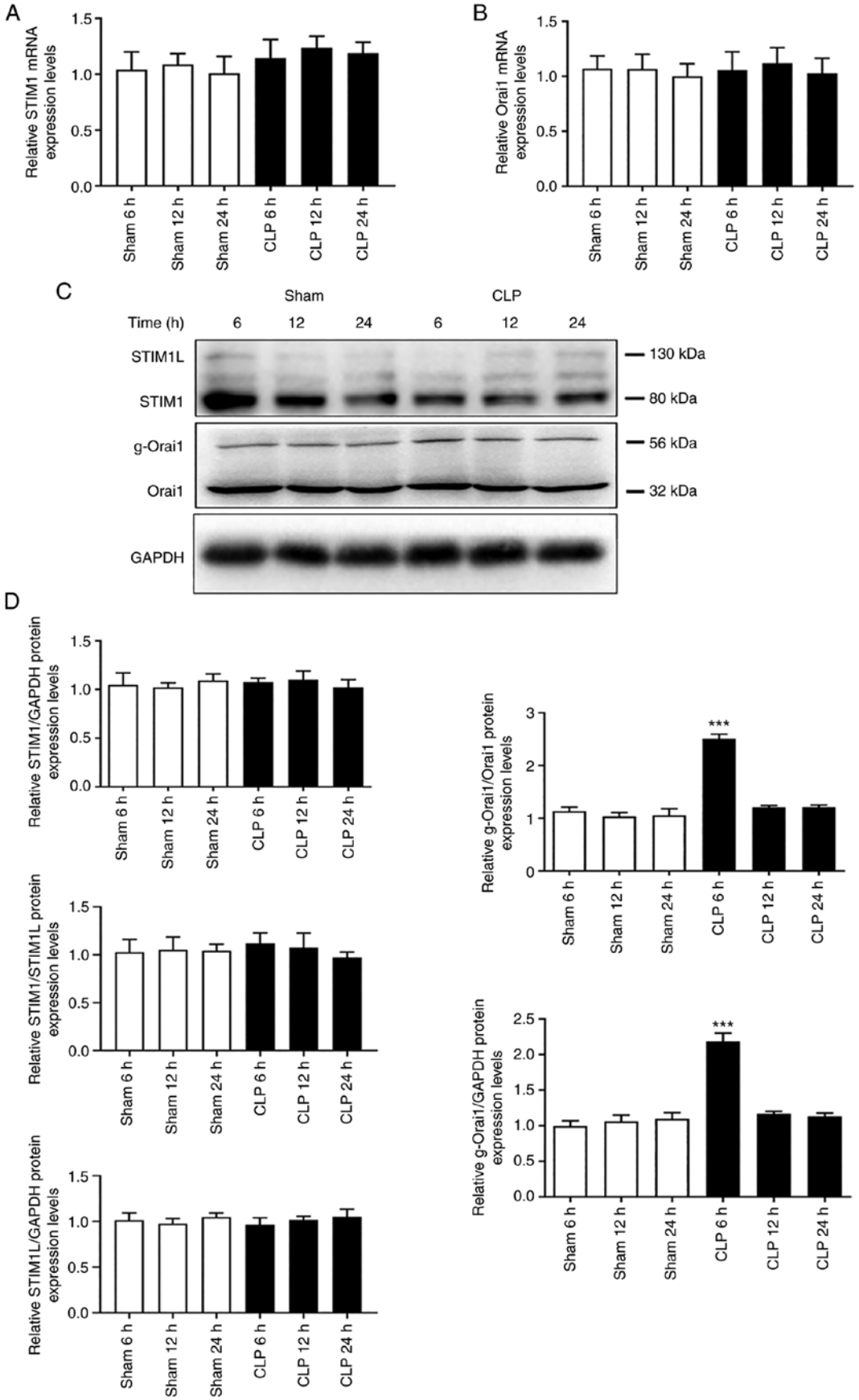

Figure 3. Increased glycosylation of Orai1 in septic mice. Myocardial tissues from septic mice that exhibited apoptotic activation were selected for STIM1 and Orai1 expression level analysis via RT-qPCR and western blotting *in vivo*. RT-qPCR was performed to analyse (A) STIM1 and (B) Orai1 mRNA expression levels. (C) Representative western blot images of cardiomyocytes from septic mice. (D) Semi-quantification of STIM1, STIM1L, Orai1 and g-Orai1 levels. Data are presented as the mean ± SEM (n=6/group). ***P<0.001 vs. sham 6 h. STIM1, stromal interaction molecule 1; STIM1L, long splice variant of STIM1; Orai1, Orai calcium release-activated calcium modulator 1; g-Orai1, glycosylation of Orai1; RT-qPCR, reverse transcription-quantitative PCR; CLP cecal ligation and puncture operation.

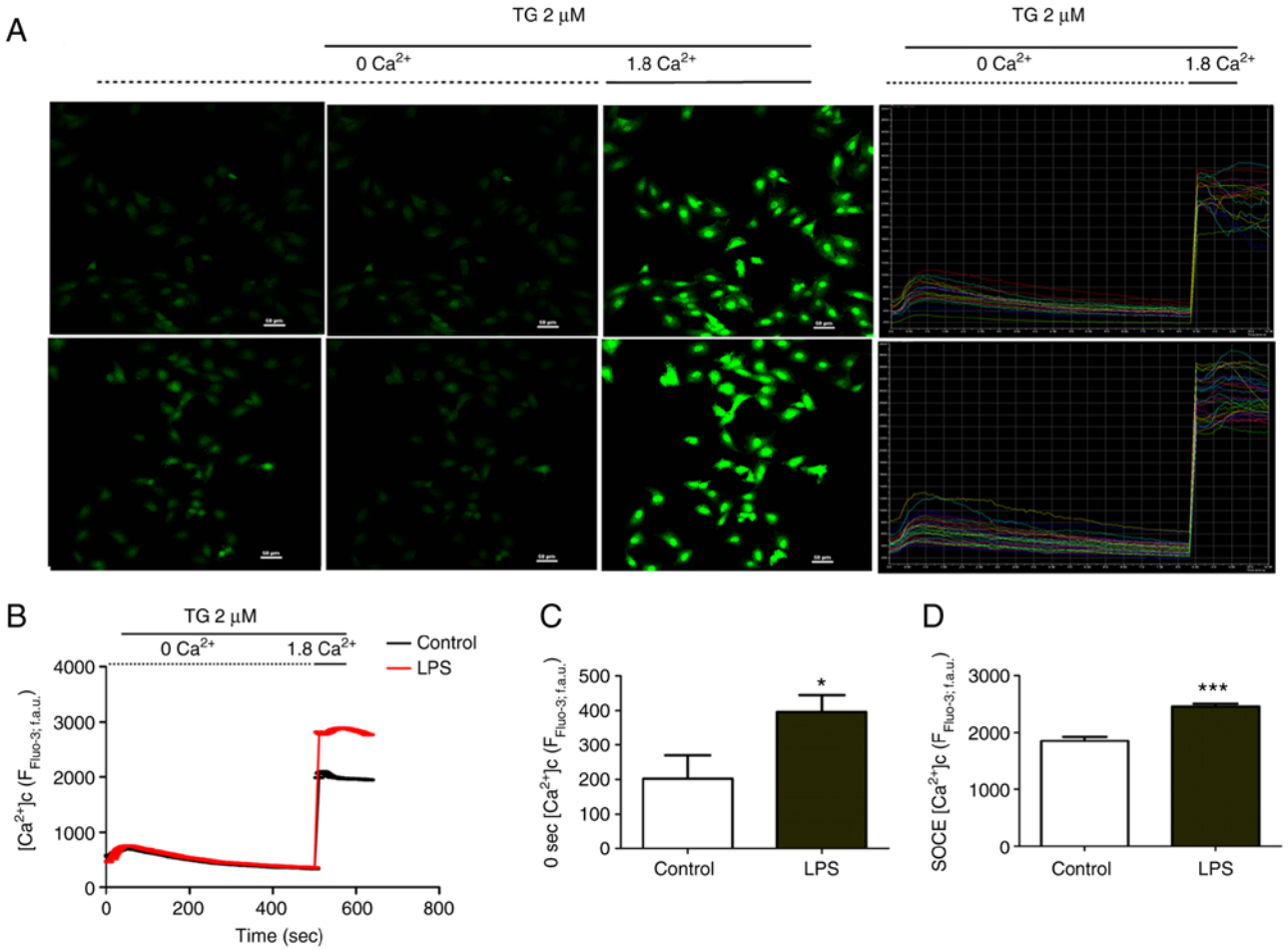

Figure 4. LPS induces increases in SOCE and the cytosolic Ca^{2+} concentration in H9C2 cells. Following loading with Fluo-3/acetoxymethyl ester, cells were administered with LPS and then washed. The images were captured using confocal microscopy before TG or Ca^{2+} was added. Real-time fluorescent images were recored every 2 sec at 488-nm excitation using confocal microscopy. (A) Representative images and traces of SOCE in H9C2 cells. Scale bar, 50 μm. (B) Quantitative analyses of the SOCE time course. (C) Quantitative analyses of SOCE changes following Ca^{2+} re-addition. (D) Quantitative analyses of the Ca^{2+} concentration before SOCE induction. Data are presented as the mean ± SEM. n>15 cells/replicate. *P<0.05 and ***P<0.001. LPS, lipopolysaccharide; SOCE, store operated Ca^{2+} entry; TG, thapsigargin; f.a.u., fluorescence arbitrary units; [Ca^{2+}]c, concentration of Ca^{2+}.

following the CLP operation and both mRNA and protein levels returned to normal at 24 h.

Orai1 glycosylation is increased in septic mice. Myocardium exhibiting apoptotic activation were obtained from septic mice to evaluate changes in STIM1 and Orai1 expression levels via RT-qPCR and western blotting. The results demonstrated that STIM1 and Orai1 mRNA and protein expression levels were not significantly different between the CLP and sham groups at 6, 12, or 24 h (Fig. 3). Interestingly, significant increases in Orai1 glycosylation were observed at 6 h after the CLP operation compared with the sham 6 h group (P<0.001).

LPS increases cytosolic Ca^{2+} levels and induces SOCE in H9C2 cells. In vitro changes in the cytosolic Ca^{2+} concentration and SOCE were observed in septic cardiomyocytes. The Ca^{2+} levels in the ER were depleted by TG in Ca^{2+}-free medium. Ca^{2+} was re-added to the medium and fluctuations in the cytosolic Ca^{2+} concentration were recorded using Fluo-3/AM fluorescence (Fig. 4A). The cytosolic Ca^{2+} concentration initially decreased before levelling off and then abruptly and markedly increased after Ca^{2+} was added to the medium. SOCE was responsible for the significant gain in fluorescence intensity after Ca^{2+} was added compared with the control (without TG or Ca^{2+}), as observed in H9C2 cells stimulated with LPS for 1-2 h (P<0.001) (Fig. 4B and C). The cytosolic Ca^{2+} concentration in H9C2 cells was also significantly enhanced following 1-2 h LPS stimulation compared with the control group (P<0.05) (Fig. 4D).

LPS-induced activation of STIM1 clustering and redistribution in H9C2 cells. Immunofluorescent staining of STIM1 was performed in H9C2 cells following LPS treatment for 30 min, 1, 2, 4 and 6 h. The distribution of STIM1 at 30 min of LPS treatment was the same as that in the control group (equivalent PBS used), although changes in the translocation of STIM1 at the ER-plasma membrane junction occurred at 1 and 2 h following LPS treatment. The distribution of STIM1 returned to normal at 4 and 6 h compared with the control group (Fig. 5A). Immunofluorescent staining of Orai1 was performed following LPS stimulation for 1 and 4 h in H9C2 cells. Immunofluorescent analysis demonstrated that LPS had no effect on the distribution and expression of Orai1 compared with the control (equivalent PBS used) (Fig. 5B).

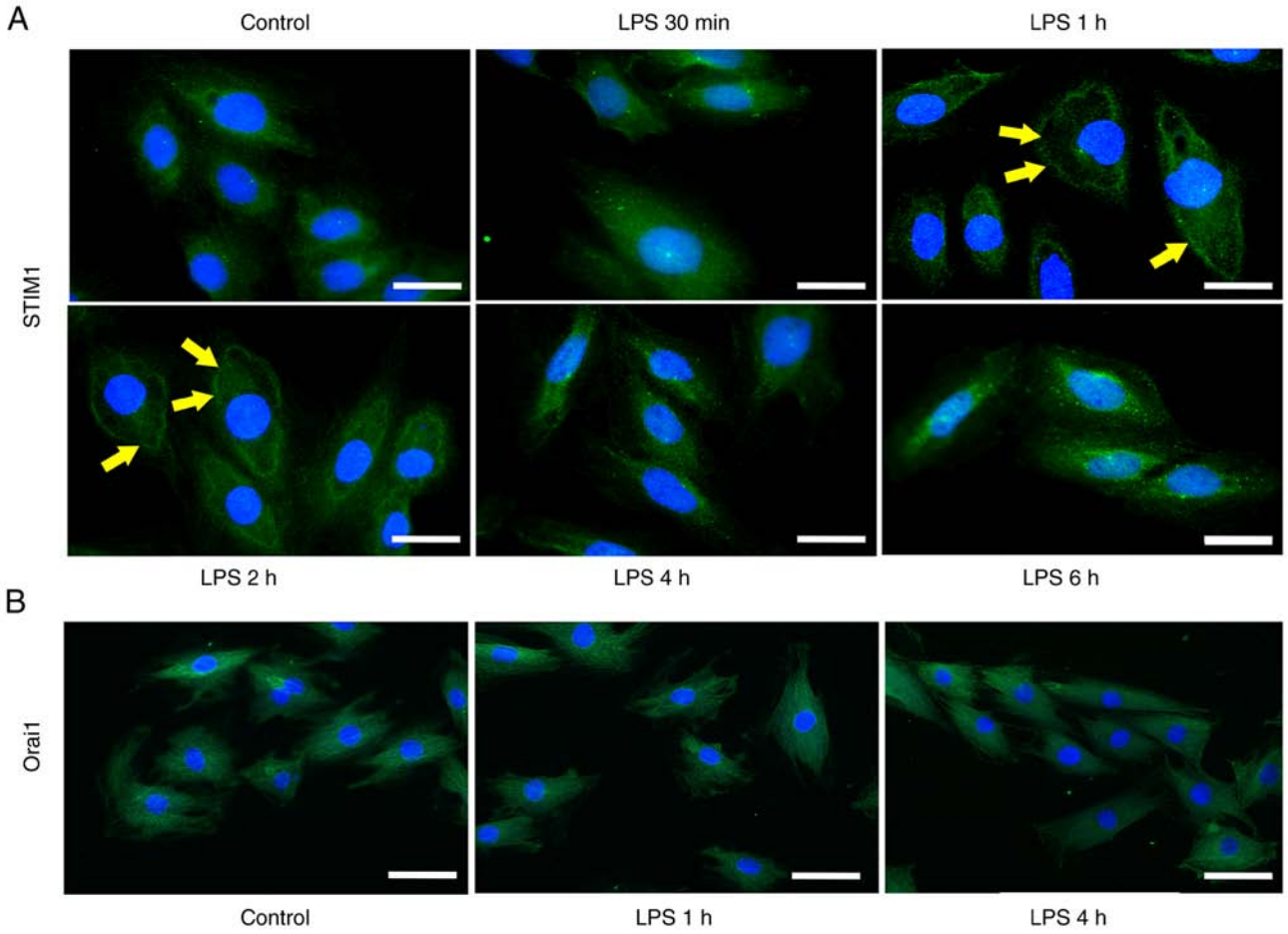

Figure 5. Activation of STIM1 in H9C2 cells stimulated with LPS. (A) Clustering and redistribution of STIM1 was visualized in H9C2 cells using immunofluorescent staining (magnification, x1,000; Scale bar, 20 μm; n=3/group). (B) Immunofluorescent staining of Orai1 in H9C2 cells (magnification, x400; n=3/group). STIM1, stromal interaction molecule 1; LPS, lipopolysaccharide; Orai1, Orai calcium release-activated calcium modulator 1.

Discussion

The present study demonstrated that myocardial dysfunction, cardiac injury and myocardial depression may be associated with increased intracellular Ca^{2+} concentrations caused by STIM1/Orai1-mediated SOCE. Cardiac contractile function was significantly reduced at 6 h and morphological changes in the cardiac tissues and the myocardial apoptosis rate were increased at 6, 12 and 24 h in the CLP compared with the corresponding sham groups. The mRNA and protein expression levels of Bax/Bcl-2 were significantly enhanced at 6 and 12 h and glycosylation of Orai1 was significantly increased at 6 h in the myocardium of septic mice. In H9C2 cells treated with LPS, we detected enhanced intracellular Ca^{2+} concentration and SOCE at 1 to 2 h and the change of clustering and distribution of STIM1 at 1, 2 h.

Septic myocardial depression occurs during the very early stage of sepsis (35). Although no consistent diagnostic criteria exist for septic myocardial dysfunction, it is clearly characterized by reduced ventricular contractility (36). Changes in ventricular contractility have been demonstrated in patients with sepsis, as well as in *in vitro* and *in vivo* experimental studies (37-39). Moreover, myocardium dystfunction in sepsis is reported to be reversable (40). Echocardiography is an irreplaceable tool for the evaluation of septic myocardial dysfunction. LVEF and LVFS are two major parameters used to assess changes in ventricular contractility. In the present study, LVEF and LVFS were reduced at 6 h following the CLP operation, before being restored at 12 h, which indicates ventricular contraction dysfunction during the early stages of sepsis and reversal of septic myocardial dysfunction. These results are in accordance with previous studies (41) and they have demonstrated the success of this animal model of septic myocardial dysfunction.

Apoptosis is a type of programmed cell death that has been demonstrated to contribute to septic myocardial depression (9). Bax and Bcl-2 belong to the Bcl-2 family of proteins associated with apoptosis and changes in these proteins over time have been observed in the heart tissue of septic animal models (41). Bcl-2 overexpression may prevent myocardial dysfunction and cardiac apoptosis in rodent models of sepsis (42). Furthermore, certain drugs and reagents have a protective effect on septic myocardial depression by inhibiting apoptosis (43-45). In the present study, the occurrence of myocardial apoptosis in sepsis was detected using TUNEL staining. The time-dependent expression (Bax/Bcl-2 was first elevated, reaching to peak, then decreased) of Bax and Bcl-2 occurred at both the mRNA and protein expression levels, which is consistent with other studies (41,42). These results further demonstrated the success of this animal model of septic myocardial injury.

The mechanisms underlying septic myocardial depression include mitochondrial dysfunction, inflammation, excessive formation of reactive oxygen species and nitric oxide, an imbalance in Ca^{2+} homeostasis and regulation of the G protein receptor kinase (46-48). In a Previous study has shown that short-term (2 min) stimulation of neonatal cardiomyocytes with septic serum was demonstrated to be sufficient to increase the basal Ca^{2+} concentration and reduce the amplitude of transient Ca^{2+} concentrations (8). An increase in the basal Ca^{2+} concentration was still detected at 24 h following stimulation; however, a reduction in the transient Ca^{2+} amplitude was not observed at this timepoint (8). These previous findings indicated that cardiac dysfunction is reversible, whereas myocardial cellular apoptosis is irreversible. Similarly, short-term (3 h) treatment of adult ventricular cardiomyocytes with LPS increases the mean cytoplasmic Ca^{2+} concentration (49). In accordance with other studies reporting an increase in the basal Ca^{2+} concentration after LPS treatment in cardiomyocytes, a significant elevation in the mean cytosolic Ca^{2+} concentration was observed in H9C2 cells stimulated with LPS for 1-2 h.

Ca^{2+} homeostasis is regulated by Ca^{2+} channels, such as LTCCs, Na^{+}/Ca^{2+} exchange channels, Orai1 and transient receptor potential canonical channels, located in the plasma membrane, as well as the ryanodine receptor and SR Ca^{2+} ATPase located in the ER membrane (29,50-52). Ca^{2+} transporters are triggered by various stimuli, including voltage changes, Ca^{2+} release and depletion of ER (53). Changes in the Ca^{2+} level in the plasma membrane may contribute to normal physiological functions, such as the contraction/relaxation cycle, the basal signalling pathway and various pathological states, such as cell structural damage, apoptosis and cell hypertrophy. Among the Ca^{2+} transporters contributing to Ca^{2+} entry, LTCCs function in transient cytoplasm Ca^{2+} cycling of the cardiomyocyte contraction/relaxation cycle. SOCE is part of the signalling pathway responsible for cell survival and death and is associated with sustained elevation of Ca^{2+} levels in the cytoplasm (18,19). The results of the present study indicated that the Ca^{2+} levels rise between 1 and 2 h in the cytoplasm, which suggested that SOCE may contribute to the occurrence and development of septic myocardial injury.

SOCE is triggered by the depletion of Ca^{2+} in the ER, which may be sensed by STIM1 and Ca^{2+} entry is activated by Ca^{2+} channels, such as Orai1 (17,54). STIM1 and Orai1 are expressed in the heart; however, their expression levels and SOCE activation are lower in adult cardiomyocytes compared with embryonic or new-born cardiomyocytes (18). This may limit investigations of STIM1/Orai1-mediated SOCE in cardiomyocytes. STIM1/Orai1-mediated SOCE was initially discovered in non-excitable cells and was thought to be absent in excitable cells (55). STIM1/Orai1-mediated SOCE was later discovered in excitable cells and was reported to contribute to hyperplasia of smooth muscle cells and hypertrophy of cardiomyocytes (20,56). However, to the best of our knowledge the role of STIM1/Orai1-mediated SOCE in myocardial injury has seldom been reported and the effect of STIM1/Orai1-mediated SOCE in septic myocardial depression has never been reported. The present study demonstrated significantly increased SOCE in cardiomyocytes stimulated by LPS, which indicated a potential relationship between SOCE and septic myocardial depression.

Slight changes in the SOCE-related proteins STIM1 and Orai1 were also observed in the present study, which differs from increased expression of STIM1 and Orai1 previously been found in the model of cardiac hypertrophy (19,57). The redistribution of STIM1 to the plasma membrane was observed for a short period following LPS stimulation and was time-dependent. Translocation of STIM1 was detected by immunofluorescence and the results indicated the oligomerized aggregation of STIM1 at the ER-plasma membrane junction. Moreover, a previous study proposed that short-term TG stimulation results in changes in the clustering and redistribution of STIM1, but not in the expression levels (19). Furthermore, two STIM1 subtypes have been reported, with STIM1L (a long splice variant of STIM1) exhibiting more prominent changes compared with STIM1 in cardiac hypertrophy models (18). In the present study two bands representing STIM1 were detected via western blotting, which corresponded to STIM1L and STIM1. However, no significant difference in the protein expression level of either STIM1L and STIM1were observed in the present study.

No change in Orai1 expression level was observed by qPCR or western blot analysis in our experiments, while a change was observed in the myocardial hypertrophy model. The plasma membrane protein Orai1 was observed at 32 kDa in most protein expression experiments. However, the SOCE rate was dependent on glycosylation of Orai1, which produced a 56 kDa marker in fibroblasts and T cells (58). In the present study the protein expression of Orai1 at both 32 and 56 kDa was detected and significant changes in Orai1 glycosylation (56 kDa) were demonstrated in the CLP group. Orai1 glycosylation was significantly increased at 6 h and returned to the baseline, which was accordance with the change in sepsis-induced cardiac dysfunction and myocardial apoptosis. Although altered expression levels of STIM1 and Orai1 were not observed in the present study, the translocation of STIM1 and significantly increased glycosylation of Orai1 indicated a potential association between STIM1/Orai1-mediated SOCE and septic myocardial depression.

In summary, the present study demonstrated that STIM1/Orai1-mediated SOCE may be associated with septic myocardial depression. Therefore, the regulation of STIM1/Orai1-mediated SOCE may have the potential to alleviate septic myocardial depression. However, further studies are needed to to confirm the exact role of STIM1/Orai1-mediated SOCE in septic cardiac depression and to determine its clinical effect and toxicity.

Acknowledgements

Not applicable.

Funding

The present study was funded by the Zhejiang Provincial Natural Science Foundation (grant no. LQ15H150003), and in part, by grants from the National Natural Science Foundation of China (grant no. 81772112 and 81871583).

Availability of data and materials

The datasets used and/or analysed during the current study are available from the corresponding author on reasonable request.

Authors' contributions

JY, ML GZ and ZL conceived and designed the study. JY, XH, QL, ZJ, SZ and GH performed the experiments and analysed the data. JY, GZ and ZL wrote the manuscript. JY, GZ, GH and ZL confirm the authenticity of all the raw data. All authors read and approved the final manuscript.

Ethics approval and consent to participate

The experiments involving animals were performed in accordance with the National Institutes of Health Guidelines for the Care and Use of Laboratory Animals and were approved by the Ethics Committee of Wenzhou Medical University (approval no. wydw2016-0217; Wenzhou, China).

Patient consent for publication

Not applicable.

Competing interests

The authors declare that they have no competing interests.

References

1. Singer M, Deutschman CS, Seymour CW, Shankar-Hari M, Annane D, Bauer M, Bellomo R, Bernard GR, Chiche JD, Coopersmith CM, *et al*: The Third International consensus definitions for sepsis and septic shock (Sepsis-3). JAMA 315: 801-810, 2016.
2. Landesberg G, Gilon D, Meroz Y, Georgieva M, Levin PD, Goodman S, Avidan A, Beeri R, Weissman C, Jaffe AS and Sprung CL: Diastolic dysfunction and mortality in severe sepsis and septic shock. Eur Heart J 33: 895-903, 2012.
3. Jeong HS, Lee TH, Bang CH, Kim JH and Hong SJ: Risk factors and outcomes of sepsis-induced myocardial dysfunction and stressinduced cardiomyopathy in sepsis or septic shock: A comparative retrospective study. Medicine (Baltimore) 97: e0263, 2018.
4. Eisner DA, Caldwell JL, Kistamás K and Trafford AW: Calcium and excitation-contraction coupling in the heart. Circ Res 121: 181-195, 2017.
5. Wang HG, Pathan N, Ethell IM, Krajewski S, Yamaguchi Y, Shibasaki F, McKeon F, Bobo T, Franke TF and Reed JC: Ca2+-induced apoptosis through calcineurin dephosphorylation of BAD. Science 284: 339-343, 1999.
6. Winslow RL, Walker MA and Greenstein JL: Modeling calcium regulation of contraction, energetics, signaling, and transcription in the cardiac myocyte. Wiley Interdiscip Rev Syst Biol Med 8: 37-67, 2016.
7. Thompson M, Kliewer A, Maass D, Becker L, White DJ, Bryant D, Arteaga G, Horton J and Giroir BP: Increased cardiomyocyte intracellular calcium during endotoxin-induced cardiac dysfunction in guinea pigs. Pediatr Res 47: 669-676, 2000.
8. Celes MR, Malvestio LM, Suadicani SO, Prado CM, Figueiredo MJ, Campos EC, Freitas AC, Spray DC, Tanowitz HB, da Silva JS and Rossi MA: Disruption of calcium homeostasis in cardiomyocytes underlies cardiac structural and functional changes in severe sepsis. PLoS One 8: e68809, 2013.
9. Suzuki J, Bayna E, Li HL, Molle ED and Lew WY: Lipopolysaccharide activates calcineurin in ventricular myocytes. J Am Coll Cardiol 49: 491-499, 2007.
10. Bers DM: Calcium fluxes involved in control of cardiac myocyte contraction. Circ Res 87: 275-281, 2000.
11. Bers DM: Calcium cycling and signaling in cardiac myocytes. Annu Rev Physiol 70: 23-49, 2008.
12. Feske S, Gwack Y, Prakriya M, Srikanth S, Puppel SH, Tanasa B, Hogan PG, Lewis RS, Daly M and Rao A: A mutation in Orai1 causes immune deficiency by abrogating CRAC channel function. Nature 441: 179-185, 2006.
13. Zitt C, Strauss B, Schwarz EC, Spaeth N, Rast G, Hatzelmann A and Hoth M: Potent inhibition of Ca2+ release-activated Ca2+ channels and T-lymphocyte activation by the pyrazole derivative BTP2. J Biol Chem 279: 12427-12437, 2004.
14. Hauser CJ, Fekete Z, Adams JM, Garced M, Livingston DH and Deitch EA: PAF-mediated Ca2+ influx in human neutrophils occurs via store-operated mechanisms. J Leukoc Biol 69: 63-68, 2001.
15. Hunton DL, Lucchesi PA, Pang Y, Cheng X, Dell'Italia LJ and Marchase RB: Capacitative calcium entry contributes to nuclear factor of activated T-cells nuclear translocation and hypertrophy in cardiomyocytes. J Biol Chem 277: 14266-14273, 2002.
16. Uehara A, Yasukochi M, Imanaga I, Nishi M and Takeshima H: Store-operated Ca2+ entry uncoupled with ryanodine receptor and junctional membrane complex in heart muscle cells. Cell Calcium 31: 89-96, 2002.
17. Shen Y, Thillaiappan NB and Taylor CW: The store-operated Ca^{2+} entry complex comprises a small cluster of STIM1 associated with one Orai1 channel. Proc Natl Acad Sci USA 118: e2010789118, 2021
18. Luo X, Hojayev B, Jiang N, Wang ZV, Tandan S, Rakalin A, Rothermel BA, Gillette TG and Hill JA: STIM1-dependent store-operated Ca^{2+} entry is required for pathological cardiac hypertrophy. J Mol Cell Cardiol 52: 136-147, 2012.
19. Hulot JS, Fauconnier J, Ramanujam D, Chaanine A, Aubart F, Sassi Y, Merkle S, Cazorla O, Ouillé A, Dupuis M, *et al*: Critical role for stromal interaction molecule 1 in cardiac hypertrophy. Circulation 124: 796-805, 2011.
20. Voelkers M, Salz M, Herzog N, Frank D, Dolatabadi N, Frey N, Gude N, Friedrich O, Koch WJ, Katus HA, *et al*: Orai1 and Stim1 regulate normal and hypertrophic growth in cardiomyocytes. J Mol Cell Cardiol 48: 1329-1334, 2010.
21. Prakriya M, Feske S, Gwack Y, Srikanth S, Rao A and Hogan PG: Orai1 is an essential pore subunit of the CRAC channel. Nature 443: 230-233, 2006.
22. Zhang SL, Yu Y, Roos J, Kozak JA, Deerinck TJ, Ellisman MH, Stauderman KA and Cahalan MD: STIM1 is a Ca2+ sensor that activates CRAC channels and migrates from the Ca2+ store to the plasma membrane. Nature 437: 902-905, 2005.
23. Luo R, Gomez AM, Benitah JP and Sabourin J: Targeting Orai1-mediated store-operated Ca^{2+} entry in heart failure. Front Cell Dev Biol 8: 586109, 2020.
24. Cacheux M, Strauss B, Raad N, Ilkan Z, Hu J, Benard L, Feske S, Hulot JS and Akar FG: Cardiomyocyte-Specific STIM1 (Stromal Interaction Molecule 1) depletion in the adult heart promotes the development of arrhythmogenic discordant alternans. Circ Arrhythm Electrophysiol 12: e007382, 2019.
25. Correll RN, Goonasekera SA, van Berlo JH, Burr AR, Accornero F, Zhang H, Makarewich CA, York AJ, Sargent MA, Chen X, *et al*: STIM1 elevation in the heart results in aberrant Ca^{2+} handling and cardiomyopathy. J Mol Cell Cardiol 87: 38-47, 2015.
26. Shiou YL, Lin HT, Ke LY, Wu BN, Shin SJ, Chen CH, Tsai WC, Chu CS and Lee HC: Very Low-density lipoproteins of metabolic syndrome modulates STIM1, suppresses store-operated calcium entry, and deranges myofilament proteins in atrial myocytes. J Clin Med 8: 881, 2019.
27. Troupes CD, Wallner M, Borghetti G, Zhang C, Mohsin S, von Lewinski D, Berretta RM, Kubo H, Chen X, Soboloff J and Houser S: Role of STIM1 (Stromal Interaction Molecule 1) in hypertrophy-related contractile dysfunction. Circ Res 121: 125-136, 2017.
28. Zheng C, Lo CY, Meng Z, Li Z, Zhong M, Zhang P, Lu J, Yang Z, Yan F, Zhang Y, *et al*: Gastrodin inhibits store-operated Ca^{2+} entry and alleviates cardiac hypertrophy. Front Pharmacol 8: 222, 2017.
29. Hobai IA, Edgecomb J, LaBarge K and Colucci WS: Dysregulation of intracellular calcium transporters in animal models of sepsis-induced cardiomyopathy. Shock 43: 3-15, 2015.
30. National Research Council (US) Committee for the Update of the Guide for the Care and Use of Laboratory Animals: Guide for the care and use of laboratory animals. 8th edition. National Academies Press (US), Washington, DC, 2011.
31. Rumienczyk I, Kulecka M, Ostrowski J, Mar D, Bomsztyk K, Standage SW and Mikula M: Multi-Organ transcriptome dynamics in a mouse model of cecal ligation and puncture-induced polymicrobial sepsis. J Inflamm Res 14: 2377-2388, 2021.
32. Gao M, Ha T, Zhang X, Liu L, Wang X, Kelley J, Singh K, Kao R, Gao X, Williams D and Li C: Toll-like receptor 3 plays a central role in cardiac dysfunction during polymicrobial sepsis. Crit Care Med 40: 2390-2399, 2012.

33. Livak KJ and Schmittgen TD: Analysis of relative gene expression data using real-time quantitative PCR and the 2(-Delta Delta C(T)) Method. Methods 25: 402-408, 2001.
34. Li M, Ye J, Zhao G, Hong G, Hu X, Cao K, Wu Y and Lu Z: Gas6 attenuates lipopolysaccharideinduced TNF-α expression and apoptosis in H9C2 cells through NF-κB and MAPK inhibition via the Axl/PI3K/Akt pathway. Int J Mol Med 44: 982-994, 2019.
35. Merx MW and Weber C: Sepsis and the heart. Circulation 116: 793-802, 2007.
36. Martin L, Derwall M, Al Zoubi S, Zechendorf E, Reuter DA, Thiemermann C and Schuerholz T: The septic heart: Current understanding of molecular mechanisms and clinical implications. Chest 155: 427-437, 2019.
37. Munt B, Jue J, Gin K, Fenwick J and Tweeddale M: Diastolic filling in human severe sepsis: An echocardiographic study. Crit Care Med 26: 1829-1833, 2018.
38. Ren J, Ren BH and Sharma AC: Sepsis-induced depressed contractile function of isolated ventricular myocytes is due to altered calcium transient properties. Shock 18: 285-288, 2002.
39. Merx MW, Liehn EA, Janssens U, Lütticken R, Schrader J, Hanrath P and Weber C: HMG-CoA reductase inhibitor simvastatin profoundly improves survival in a murine model of sepsis. Circulation 109: 2560-2565, 2004.
40. Wang H, Bei Y, Shen S, Huang P, Shi J, Zhang J, Sun Q, Chen Y, Yang Y, Xu T, *et al*: MiR-21-3p controls sepsis-associated cardiac dysfunction via regulating SORBS2. J Mol Cell Cardiol 94: 43-53, 2016.
41. McDonald TE, Grinman MN, Carthy CM and Walley KR: Endotoxin infusion in rats induces apoptotic and survival pathways in hearts. Am J Physiol Heart Circ Physiol 279: H2053-H2061, 2000.
42. Lancel S, Petillot P, Favory R, Stebach N, Lahorte C, Danze PM, Vallet B, Marchetti P and Neviere R: Expression of apoptosis regulatory factors during myocardial dysfunction in endotoxemic rats. Crit Care Med 33: 492-496, 2005.
43. Li Z, Yi N, Chen R, Meng Y, Wang Y, Liu H, Cao W, Hu Y, Gu Y, Tong C, *et al*: miR-29b-3p protects cardiomyocytes against endotoxin-induced apoptosis and inflammatory response through targeting FOXO3A. Cell Signal 74: 109716, 2020.
44. Liu L, Yan M, Yang R, Qin X, Chen L, Li L, Si J, Li X and Ma K: Adiponectin attenuates lipopolysaccharide-induced apoptosis by regulating the Cx43/PI3K/AKT pathway. Front Pharmacol 12: 644225, 2021.
45. Su ZD, Wei XB, Fu YB, Xu J, Wang ZH, Wang Y, Cao JF, Huang JL and Yu DQ: Melatonin alleviates lipopolysaccharide-induced myocardial injury by inhibiting inflammation and pyroptosis in cardiomyocytes. Ann Transl Med 9: 413, 2021.
46. Ravikumar N, Sayed MA, Poonsuph CJ, Sehgal R, Shirke MM and Harky A: Septic cardiomyopathy: From basics to management choices. Curr Probl Cardiol 46: 100767, 2021.
47. Liu YC, Yu MM, Shou ST and Chai YF: Sepsis-Induced cardiomyopathy: Mechanisms and treatments. Front Immunol 8: 1021, 2017.
48. Dal-Secco D, DalBó S, Lautherbach NES, Gava FN, Celes MRN, Benedet PO, Souza AH, Akinaga J, Lima V, Silva KP, *et al*: Cardiac hyporesponsiveness in severe sepsis is associated with nitric oxide-dependent activation of G protein receptor kinase. Am J Physiol Heart Circ Physiol 313: H149-H163, 2017.
49. Wang Y, Wang Y, Yang D, Yu X, Li H, Lv X, Lu D and Wang H: β_1-adrenoceptor stimulation promotes LPS-induced cardiomyocyte apoptosis through activating PKA and enhancing CaMKII and IκBα phosphorylation. Crit Care 19: 76, 2015.
50. Gavali JT, Carrillo ED, García MC and Sánchez JA: The mitochondrial K-ATP channel opener diazoxide upregulates STIM1 and Orai1 via ROS and the MAPK pathway in adult rat cardiomyocytes. Cell Biosci 10: 96, 2020.
51. Numaga-Tomita T and Nishida M: TRPC channels in cardiac plasticity. Cells 9: 454, 2020.
52. Johnson MT, Gudlur A, Zhang X, Xin P, Emrich SM, Yoast RE, Courjaret R, Nwokonko RM, Li W, Hempel N, *et al*: L-type Ca^{2+} channel blockers promote vascular remodeling through activation of STIM proteins. Proc Natl Acad Sci USA 117: 17369-17380, 2020.
53. Collins HE, Zhu-Mauldin X, Marchase RB and Chatham JC: STIM1/Orai1-mediated SOCE: Current perspectives and potential roles in cardiac function and pathology. Am J Physiol Heart Circ Physiol 305: H446-H458, 2013.
54. Lewis RS: Store-Operated calcium channels: From function to structure and back again. Cold Spring Harb Perspect Biol 12: a035055, 2020.
55. Putney JW Jr: A model for receptor-regulated calcium entry. Cell Calcium 7: 1-12, 1986.
56. Climent B, Santiago E, Sánchez A, Muñoz-Picos M, Pérez-Vizcaíno F, García-Sacristán A, Rivera L and Prieto D: Metabolic syndrome inhibits store-operated Ca^{2+} entry and calcium-induced calcium-release mechanism in coronary artery smooth muscle. Biochem Pharmacol 182: 114222, 2020.
57. Segin S, Berlin M, Richter C, Flockerzi RMV, Worley P, Freichel M and Londoño JEC: cardiomyocyte-specific deletion of orai1 reveals its protective role in angiotensin-II-induced pathological cardiac remodeling. Cells 9: 1092, 2020.
58. Kappel S, Borgström A, Stokłosa P, Dörr K and Peinelt C: Store-operated calcium entry in disease: Beyond STIM/Orai expression levels. Semin Cell Dev Biol 94: 66-73, 2019.